# Supplementary Information

# New insights in the polydopamine formation *via* surface adsorption

*Hamoon Hemmatpour[1,2], Oreste De Luca[1*], Dominic Crestani[1], Alessia Lasorsa[1], Patrick C.A. van der Wel[1], Katja Loos[1], Theodosis Giousis[1,3], Vahid Haddadi Asl[2] and Petra Rudolf[1*]*

1 Zernike Institute for Advanced Materials, University of Groningen, Nijenborgh 4, 9747AG Groningen, the Netherlands

2 Department of Polymer Engineering and Color Technology, Amirkabir University of Technology, P.O. Box 1587-4413, Tehran, Iran

3 Department of Materials Science & Engineering, University of Ioannina, 45110, Ioannina, Greece.

*Corresponding authors. Email: oreste.deluca89@gmail.com, p.rudolf@rug.nl

## Supplementary Figures

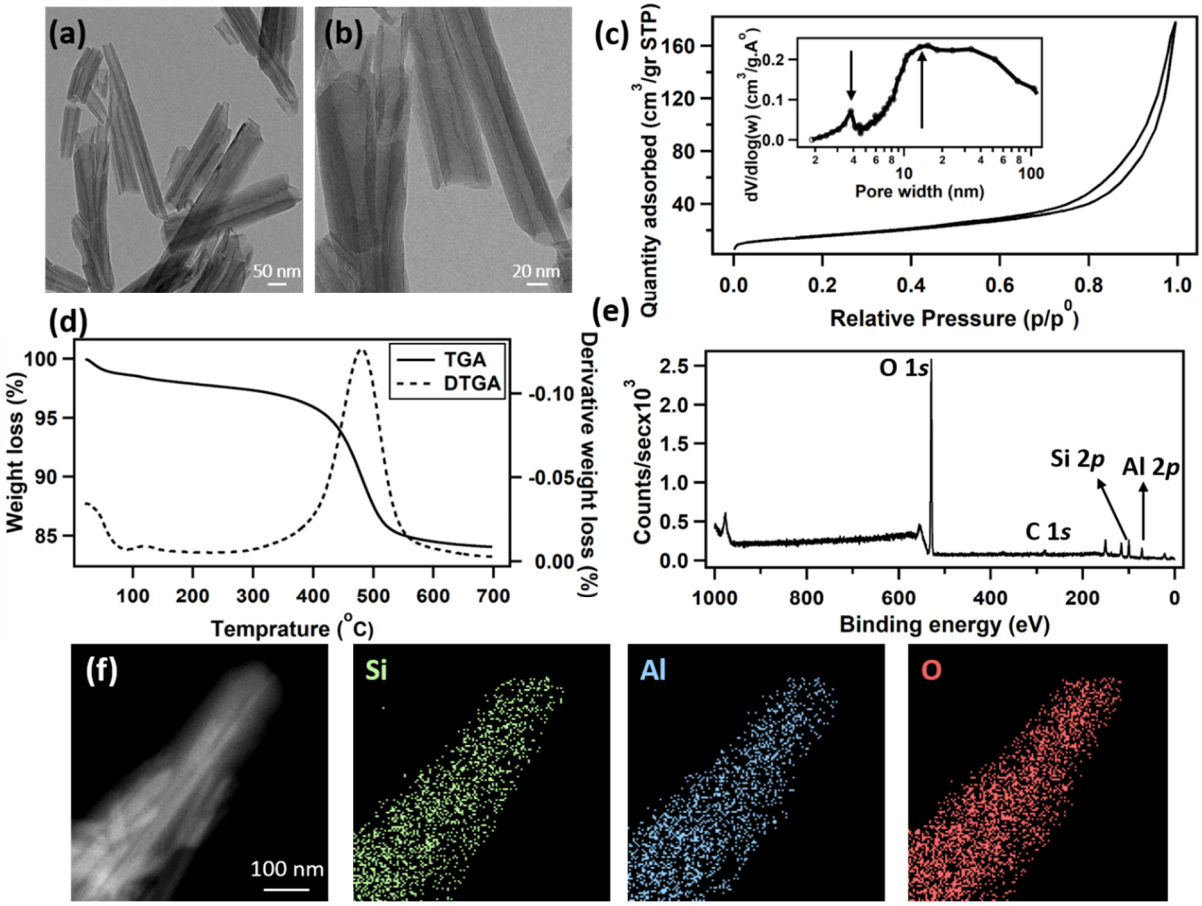


**Supplementary Figure 1.** Characterization of pristine halloysite nanotubes. (a and b) Transmission electron microscopy images, (c) $N_2$ adsorption/desorption isotherm; inset: pore size distribution, (d) thermogravimentric and differential thermogravimetric analysis, (e) X-ray photoelectron spectroscopy wide scan spectra and (f) elemental mapping images from energy dispersive X-ray spectroscopy.

As seen in the transmission electron microscopy (TEM) images in Fig. 1a-b, the HNTs used in this study have an open-ended tubular structure with an inner diameter of 5 - 20 nm, an outer diameter range from 50 to 100 nm and a length in the range of 0.5 – 1.5 µm. To learn about their porosity, $N_2$ adsorption and desorption was analyzed, and as shown in Fig. 1c, the isotherm of HNT can be categorized as type IV according to the IUPAC classification, which points to a mesoporous structure.[1] BET analysis showed that the HNT surface area and total pore volume are 46.6 $m^2/g$ and 0.28 $cm^3/g$, respectively. Such relatively high surface area and large pore volume make HNT an ideal candidate as sorbent of a vast variety of molecules.[2] When examining the logarithmic pore size distribution deduced from the desorption branch of the $N_2$ isotherm based on the Barrett, Joyner, and Halenda model (see inset in Fig. 1c), two main pore size distributions can be distinguished; the first peak centered at 3.5 nm is assigned to the longitudinal slit-shaped pores on the outer surface of HNTs. According to Koyama and co-workers[3], such mesopores form during the dehydration process when the rolled-up layers of the tubular halloysite separate. The second wide pore size distribution between 6 and 100

nm comprises two different structural features; the shoulder centered at 15 nm is assigned to the cavity inside the nanotubes, while the macropores in the range of >50 nm relate to the randomly arranged empty spaces outside the nanotubes, formed when they agglomerate into bundles. When the thermal decomposition of HNTs was studied by thermogravimetric analysis (TGA), we found a two-step thermal decomposition behavior (see Fig. 1d); in the first step, occurring at temperatures between 100 and 150 °C, the residual water intercalated in the HNT interlayer space is removed, resulting in a small weight loss of about 1 wt.%. The second step from 400 to 600 °C is due to the dihydroxylation of Al-OH groups on the HNTs' inner surfaces[4] and results in a weight loss of about 13.6 wt.%. The chemical composition of HNT was investigated by X-ray photoelectron spectroscopy (XPS) and elemental mapping through energy dispersive X-ray spectroscopy (EDS) and the results are presented in Fig. 1e and Fig. 1f, respectively. The XPS survey scan shows the signatures of the elements expected for aluminosilicate, *i.e.* O, Si and Al; in addition, a small feature typical of adventitious carbon is observed.[4] Stoichiometric analysis of the detailed core level XPS data reveals that the Si/Al atomic ratio is 1.1±0.1, in good agreement, within the experimental uncertainty, with the chemical formula of HNT. The homogenous distribution of Si, Al and O over an individual HNT was confirmed by EDS elemental mapping (see Fig. 1f). Furthermore, the carbon signal was not detected on the individual nanotube.

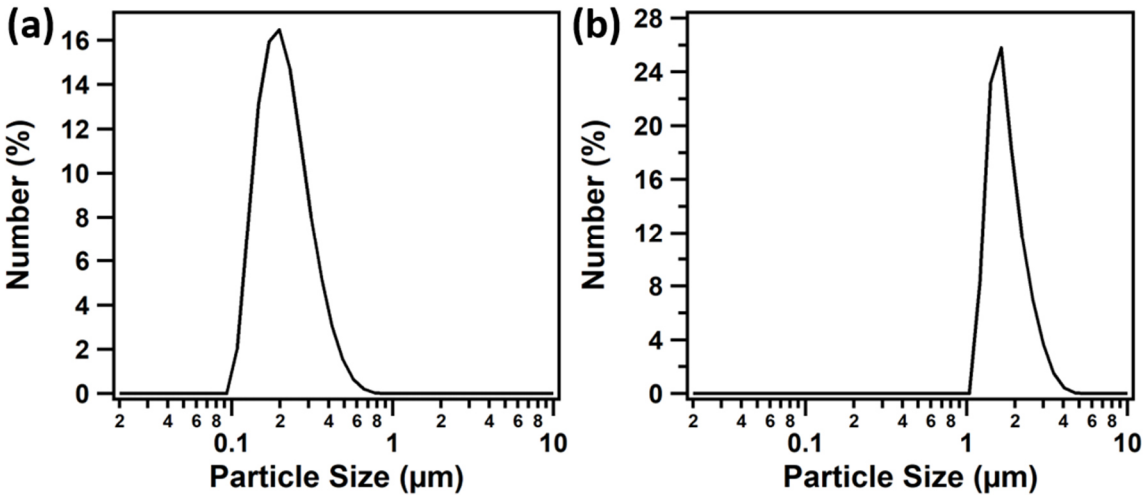


**Supplementary Figure 2.** Particle size distribution as deduced from dynamic light scattering of halloysite nanotubes dispersed in Milli-Q water (a) before and (b) after adding dopamine.

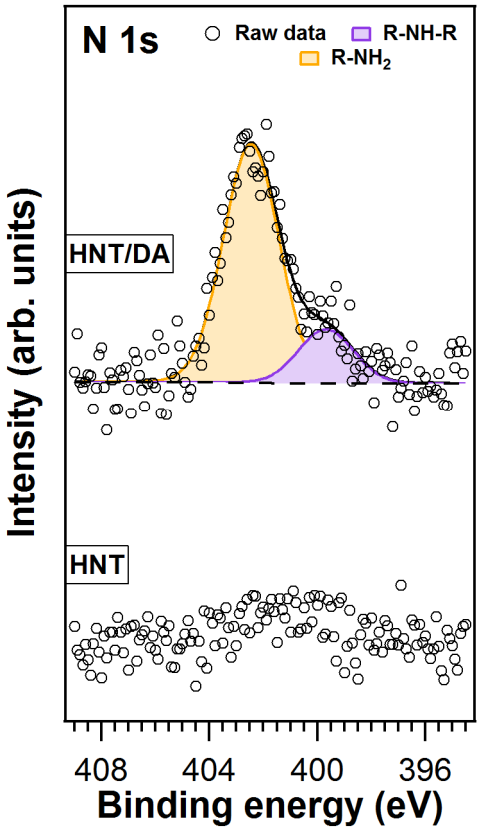


**Supplementary Figure 3.** XPS spectra of N1s core level region before and after dopamine adsorption on HNTs.

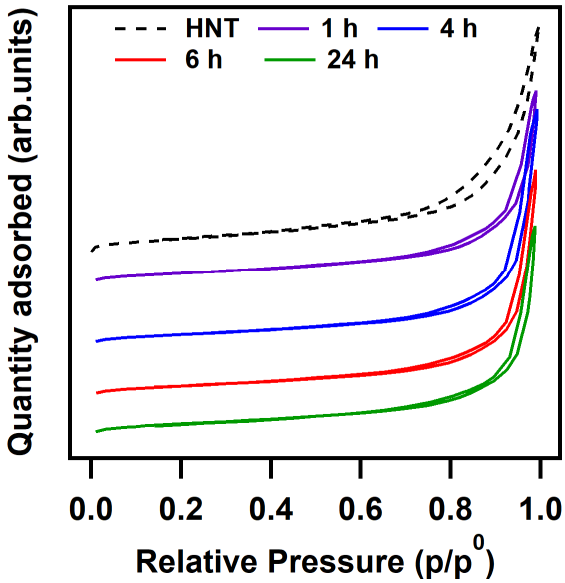


**Supplementary Figure 4.** $N_2$ adsorption/desorption isotherms for HNT-PDA after different polymerization times.

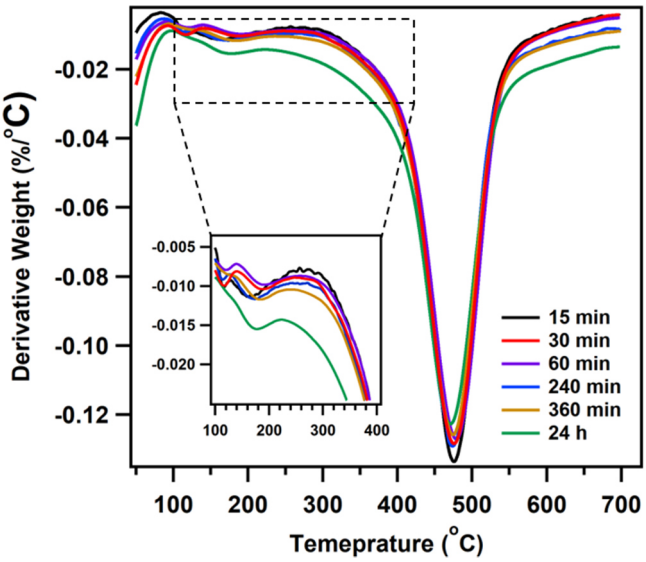


**Supplementary Figure 5.** Derivative thermogravimetric graphs for HNT-PDA after different polymerization times.

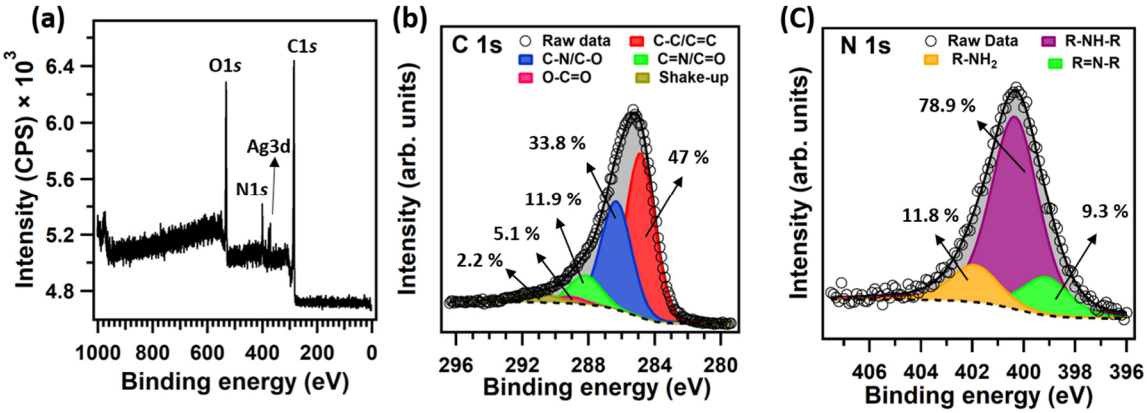


**Supplementary Figure 6.** X-ray photoelectron spectroscopy: (a) wide scan spectrum, (b) C1s and (c) N1s core-level regions of PDA-A.

To have a reference, we first investigated by XPS the surface chemical composition of the PDA-A samples, isolated from an aqueous alkaline dopamine solution after 24 h. The results are shown in Fig. 6; carbon, nitrogen and oxygen in respectively atomic percentages of 70.5, 22.1 and 7.4 at.% were identified as the main constituents of PDA-A sample. The doublet signal located at binding energies (BE) of 373.8 and 367.8 eV is respectively attributed to the Ag3$d_{3/2}$ and Ag3$d_{5/2}$ core levels from the silver substrate, which was used as a support for mounting the samples (Fig. 6a). The C1*s* spectrum (in Fig. 6b) exhibits an asymmetrical shape, which requires five components to obtain a good fit. The peak at a BE of 284.8 eV (marked in red) can be assigned to C-C/C=C species, while the other components located at 286.1 eV, 287.5, 289.2 eV can be ascribed to C-O/C-N (blue), C=O/C=N (green) and O=C-O (pink) bonds, respectively[5,6]. The peak at about 291.3 eV is assigned to the shake-up component[7]. The presence of the carbonyl functional group indicates that a portion of the catechol groups in

dopamine units converted to quinone groups upon auto-oxidation, as already reported in previous studies[8]. Moreover, the presence of the O=C-O component in the C1*s* core level region confirms the oxidative breakage of the quinone rings by the $H_2O_2$ formed *in situ*, resulting in the formation of pyrrole carboxylic acid moieties (PDCA)[9]. The N1*s* spectrum (Fig. 6c) evidences the presence of three chemical environments for nitrogen atoms. The predominant peak, located at a BE of 400.3 eV is attributed to the secondary amine moieties (R-NH-R, marked in purple), while the two less intense components located at BEs of 402.0 and 399.0 eV are assigned to primary amine (R-$NH_2$, orange) and imine (R=N-R, green) functional groups, respectively[7]. Considering the most proposed building blocks for PDA, primary amine corresponds to both DA and DAQ, secondary amine is associated with DAC, DHI and PDCA and imine is associated with the tautomeric species, TS (see Fig. 4 in the main text). The predominance of the secondary amine species points out the crucial role of the conversion of dopamine molecules into the reaction intermediates and tautomeric species by oxidation and cyclization, in agreement with the previously reported mechanism for the PDA formation[8,10].

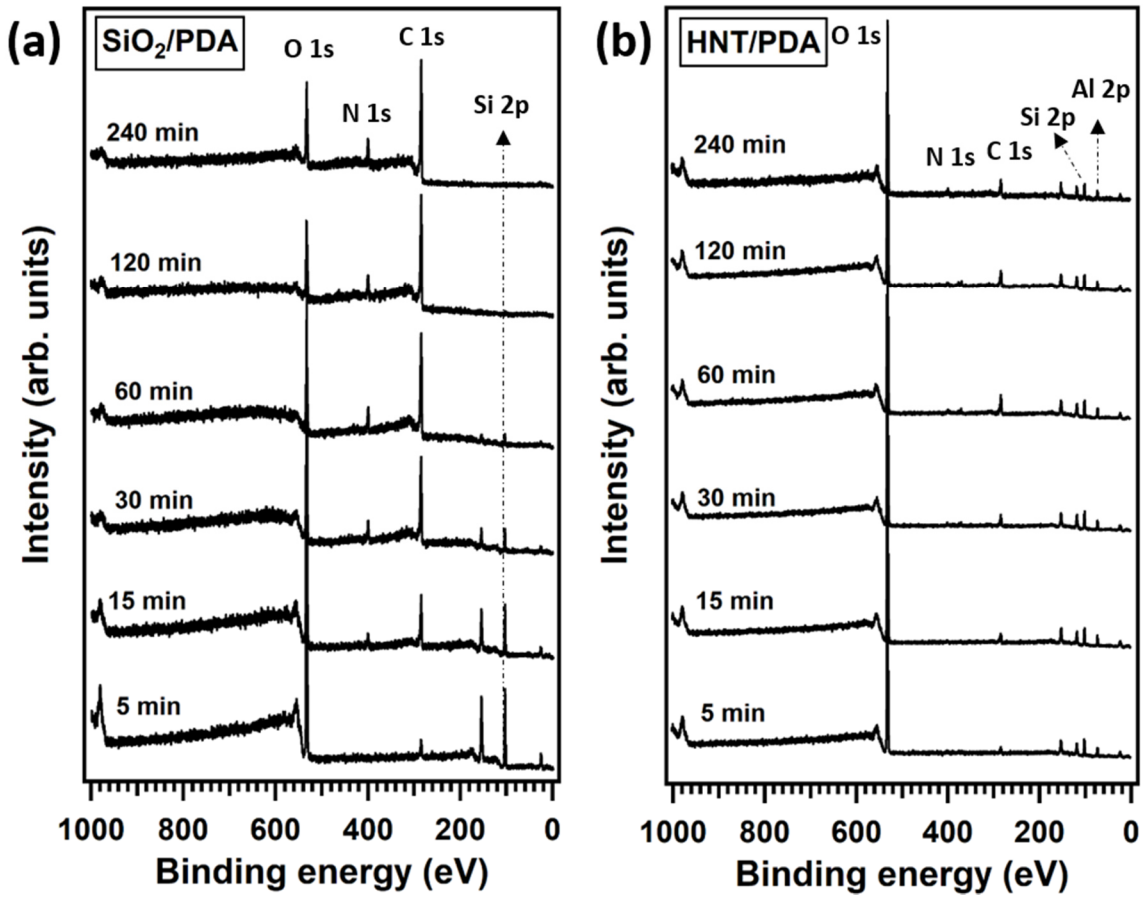


**Supplementary Figure 7.** X-ray photoelectron spectroscopy: wide scan surveys for a PDA layer deposited on $SiO_2$ (a) and HNTs (b)after different dopamine polymerization times.

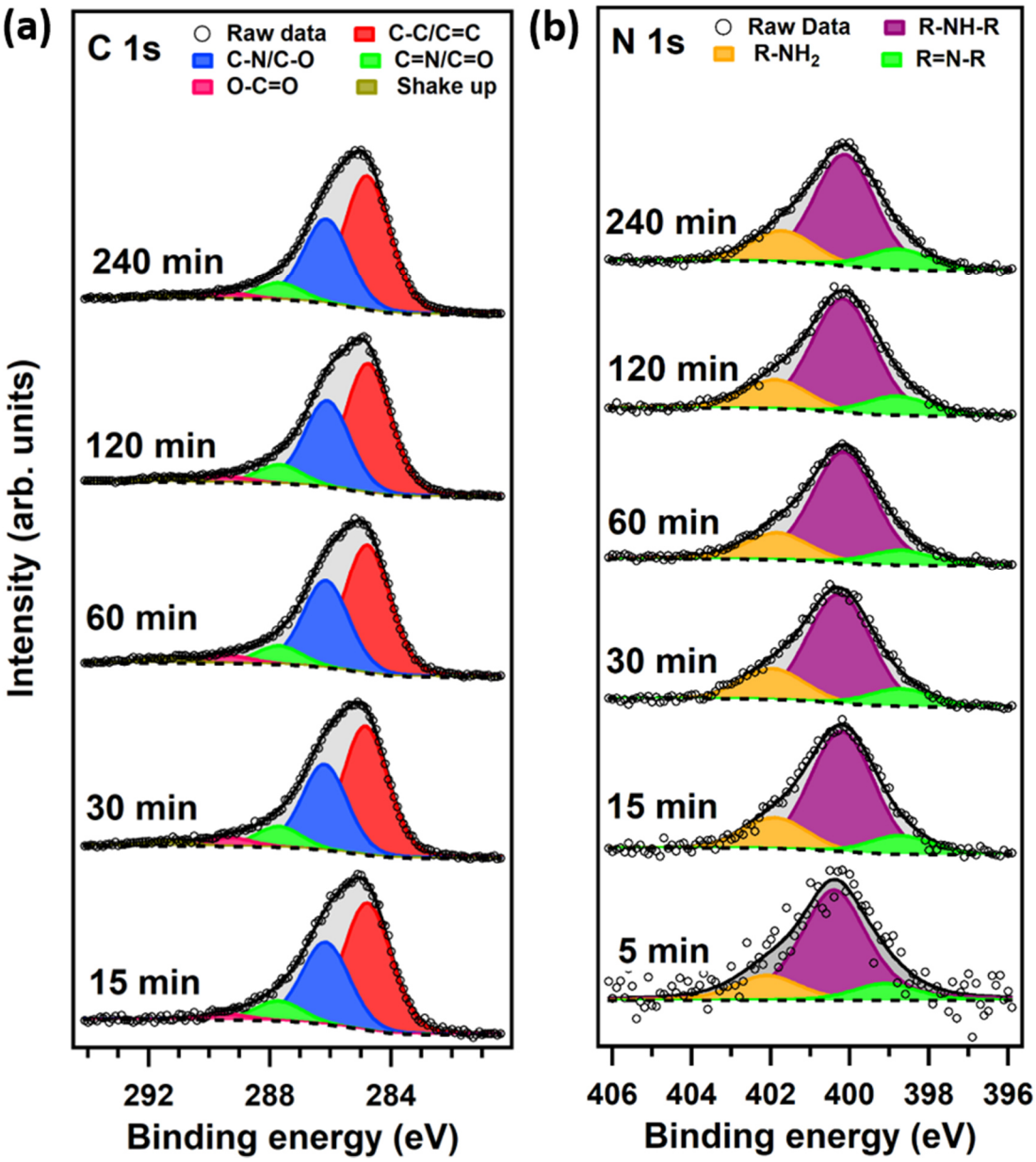


**Supplementary Figure 8.** XPS High-resolution spectra of C1*s* and N1*s* core level regions of the PDA layer deposited on a $SiO_2$ substrate after different deposition times.

## Supplementary Tables

**Supplementary Table 1.** Chemical composition (in at.%) of $SiO_2$-PDA and HNT-PDA after different polymerization times and corresponding N/C ratio.

| Polymerization time (min) | Chemical composition (in at.%) | | | | | | | | | | |
|---|---|---|---|---|---|---|---|---|---|---|---|
| | $SiO_2$-PDA | | | | | HNT-PDA | | | | | |
| | C | N | O | Si | N/C | C | N | O | Al | Si | N/C |
| 5 | 7.5 | 0.7 | 63.1 | 28.7 | 0.09 | 7.2 | 0.9 | 64.4 | 13 | 14.3 | 0.12 |
| 15 | 27.9 | 3.1 | 47.7 | 21.3 | 0.11 | 9.5 | 1 | 63.3 | 12 | 14.2 | 0.10 |
| 30 | 55.0 | 5.9 | 28.4 | 10.7 | 0.11 | 11 | 1.2 | 62.1 | 11.7 | 14 | 0.11 |
| 60 | 66.7 | 8.0 | 21.0 | 4.3 | 0.12 | 15.8 | 1.5 | 58 | 11.4 | 13.3 | 0.09 |
| 120 | 71.6 | 7.9 | 19.5 | 1.0 | 0.11 | 15.3 | 1.6 | 60 | 10.5 | 12.6 | 0.10 |
| 240 | 73.5 | 8.1 | 18.4 | 0 | 0.11 | 17.4 | 2 | 60.1 | 9.5 | 11 | 0.11 |

**Supplementary Table 2.** Relative contribution (in %) of the different functional groups to the total spectral intensities of the C1*s* and N1*s* photoemission lines of the PDA layer deposited on the $SiO_2$ substrate at different deposition times.

| Deposition time (min) | C1*s* | | | | | N1*s* | | |
|---|---|---|---|---|---|---|---|---|
| | C-C,C=C | C-N,C-O | C=O,C=N | O=C-C | Shake-up | $R\text{-}NH_3^+$ | R-NH-R | R=N-R |
| 5 | 50.2 | 37.4 | 10.9 | 1.5 | 0 | 16.6 | 72.1 | 11.3 |
| 15 | 54.0 | 35.0 | 8.5 | 2.5 | 0 | 18.3 | 70.7 | 11.0 |
| 30 | 51.6 | 34.4 | 8.5 | 3.6 | 2.1 | 19.7 | 69.1 | 11.2 |
| 60 | 51.8 | 35.2 | 7.6 | 3.2 | 2.1 | 17.8 | 72.4 | 9.8 |
| 120 | 53.3 | 35.4 | 7.5 | 2.3 | 1.4 | 18.1 | 70.0 | 11.9 |
| 240 | 55.0 | 34.8 | 7.0 | 2.2 | 1.1 | 19.1 | 68.1 | 12.8 |

**Supplementary Table 3.** Numbers of chemical species in each building block of polydopamine

| Molecule | Chemical Species | | | | | | |
|---|---|---|---|---|---|---|---|
| | C-C/C=C | C-O/C-N | C=O/C=N | O-C=O | R-NH-R | R-$NH_3^+$ | R=N-R |
| Dopamine (DA) | 5 | 3 | 0 | 0 | 0 | 1 | 0 |
| Dopamine quinone (DAQ) | 5 | 1 | 2 | 0 | 0 | 1 | 0 |
| Dopaminechrome (DAC) | 4 | 2 | 2 | 0 | 1 | 0 | 0 |
| Tris | 0 | 4 | 0 | 0 | 0 | 1 | 0 |
| Pyrrole dicarboxylic acid (PDCA) | 2 | 2 | 0 | 2 | 1 | 0 | 0 |
| Tautomeric structure (TS) | 4 | 2 | 2 | 0 | 0 | 0 | 1 |

$$\frac{5\,DA + 5\,DAQ + 4\,DAC + 2\,PDCA + 4\,TS}{3\,DA + 1\,DAQ + 2\,DAC + 4\,Tris + 2\,PDCA + 2\,TS} = \frac{C{-}C, C{=}C}{C{-}O, C{-}N} \quad (1)$$

$$\frac{3\,DA + 1\,DAQ + 2\,DAC + 4\,Tris + 2\,PDCA + 2\,TS}{2\,DAQ + 2\,DAC + 2\,TS} = \frac{C{-}O, C{-}N}{C{=}O, C{=}N} \quad (2)$$

$$\frac{3\,DA + 1\,DAQ + 2\,DAC + 4\,Tris + 2\,PDCA + 2\,TS}{2\,PDCA} = \frac{C{-}O, C{-}N}{O{-}C{=}O} \quad (3)$$

$$\frac{DAC + PDCA}{DA + DAQ + Tris} = \frac{R{-}NH{-}R}{R{-}NH_3^+} \quad (4)$$

$$\frac{TS}{DA + DAQ + Tris} = \frac{R{=}N{-}R}{R{-}NH_3^+} \quad (5)$$

$$DA + DAC + DAQ + Tris + PDCA + TS = 1 \quad (6)$$

**Empirical model developed based on the X-ray photoelectron spectroscopy data**

To evaluate the percentage of each building block during the dopamine polymerization, a numerical method was used. By taking into account the number of the chemical species present in each building block structure (see Fig. 4 in the main text and Supplementary Table 3) the left side of the equations 1 to 6 were developed, while for the right side the ratios were obtained from the relative intensities of the various chemical groups in the high-resolution spectra of the C1*s* and N1*s* core level regions; the partial presence of each building block is shown by the representative abbreviations. Specifically, considering equation (1), the right hand side corresponds to the ratio between the spectral intensities of the C-C/C=C species (marked in red in Fig. 5 of the main text) and that of the C-O/C-N (blue in Fig. 5 main text). The six equations system was solved simultaneously, using a linear equations solver for six

variables for each of the polymerization times for which we had collected XPS data and the results are summarized in Supplementary Table 4.

**Supplementary Table 4.** Evolution of the building blocks in HNT-PDA (in %) as a function of polymerization time.

| Building blocks | Polymerization time (min) | | | | | |
|---|---|---|---|---|---|---|
| | 5 | 15 | 30 | 60 | 120 | 240 |
| Dopamine (DA) | 0 | 3.0 | 18.6 | 18.5 | 13.0 | 7.4 |
| Dopamine quinone (DAQ) | 30.6 | 17.5 | 12.9 | 2.1 | 4.3 | 0 |
| Dopaminechrome (DAC) | 11.6 | 23.0 | 18.1 | 26.4 | 32.7 | 44.0 |
| Tris | 48.2 | 44.0 | 31.7 | 27.2 | 26.8 | 24.0 |
| Pyrrole dicarboxylic acid (PDCA) | 9.6 | 12.5 | 12.2 | 19.0 | 16.1 | 15.0 |
| Tautomeric structure (TS) | 0 | 0 | 6.5 | 6.8 | 7.1 | 9.6 |

**Supplementary Table 5.** Comparison of the ratios between chemical species as deduced from the XPS data and as predicted by the model.

| HNT-PDA samples | Chemical species ratio | | | |
|---|---|---|---|---|
| | C-C, C=C/C=O, C=N | | C-C,C=C/O-C=O | |
| | Model | Experimental Data | Model | Experimental data |
| 5 min | 2.6 | 2.0 | 11.4 | 11.4 |
| 15 min | 2.7 | 2.4 | 8.8 | 8 |
| 30 min | 3.7 | 3.8 | 11.5 | 11.3 |
| 60 min | 3.9 | 3.8 | 7.2 | 7.1 |
| 120 min | 3.1 | 3.1 | 8.6 | 8.5 |
| 240 min | 2.6 | 2.7 | 9.4 | 9.1 |

Supplementary Table 5 shows a comparison of the ratios between different chemical species, which were not taken into account in equations 1 to 6, calculated based on experimental data versus those predicted by the model. One clearly sees that the experimental data match well with the model, and hence validate it.

## References


1. Lim, S. et al. Modification of halloysite nanotubes for enhancement of gas-adsorption capacity. *Clays Clay Miner.* **68,** 189-196 (2020).
2. Wan, X. et al. Core@ double-shell structured magnetic halloysite nanotube nano-hybrid as efficient recyclable adsorbent for methylene blue removal. *Chem. Eng. J.* **330,** 491-504 (2017).
3. Kohyama, N. et al. Observation of the hydrated form of tubular halloysite by an electron microscope equipped with an environmental cell. *Clays Clay Miner.* **26,** 25-40 (1978).
4. Hemmatpour, H. et al. Synthesis of pH-sensitive poly (N, N-dimethylaminoethyl methacrylate)-grafted halloysite nanotubes for adsorption and controlled release of DPH and DS drugs. *Polymer* **65,** 143-153 (2015).
5. Ding, Y. et al. Insights into the aggregation/deposition and structure of a polydopamine film. *Langmuir* **30,** 12258-12269 (2014).
6. Feng, J. et al. Characterizations of the formation of polydopamine-coated halloysite nanotubes in various pH environments. *Langmuir* **32,** 10377-10386 (2016).
7. Zangmeister, R. A. et al. Characterization of polydopamine thin films deposited at short times by autoxidation of dopamine. *Langmuir* **29,** 8619-8628 (2013).
8. Liebscher, J. Chemistry of polydopamine–scope, variation, and limitation. *Eur. J. Org. Chem*. **2019,** 4976-4994 (2019).
9. Cheng, W. et al. Versatile polydopamine platforms: synthesis and promising applications for surface modification and advanced nanomedicine. ACS Nano **13,** 8537-8565 (2019).
10. Lyu, Q. et al. Unravelling the polydopamine mystery: is the end in sight? *Polym. Chem.* **10,** 5771-5777 (2019)